Efficiency enhancement of a two-beam free-electron laser using a nonlinearly tapered wiggler

Maryam Zahedian, B. Maraghechi†, and M.H. Rouhani

Department of Physics, Amirkabir University of Technology, P.O. Box 15875-4413, *Tehran, Iran*

(Received 2 August 2011; revised manuscript received 6 September 2011)

A nonlinear and non-averaged model of a two-beam free-electron laser (FEL) wiggler that is tapered nonlinearly in the absence of slippage is presented. The two beams are assumed to have different energies, and the fundamental resonance of the higher energy beam is at the third harmonic of the lower energy beam. By using Maxwell's equations and the full Lorentz force equation of motion for the electron beams, coupled differential equations are derived and solved numerically by the fourth-order Runge–Kutta method. The amplitude of the wiggler field is assumed to decrease nonlinearly when the saturation of the third harmonic occurs. By simulation, the optimum starting point of the tapering and the slopes for reducing the wiggler amplitude are found. This technique can be applied to substantially improve the efficiency of the two-beam FEL in the XUV and X-ray regions. The effect of tapering on the dynamical stability of the fast electron beam is also studied.

Keywords: free-electron lasers, harmonic generation, Kolmogorov entropy, efficiency enhancement

PACS: 41.60.Cr, 42.65.Ky, 02.60.Cb, 94.20.wj **DOI:** 10.1088/1674-1056/21/3/034101

1. Introduction

There is considerable interest in the production of coherent high-power short-wavelength radiation in the X-ray region. The interest in X-ray free electron lasers (FELs) has encouraged the researchers to test the basic physics and technology by using experiments at longer wavelengths.[1] The X-ray FEL is favorable compared to the high-power optical laser because the diffraction limit is three orders of magnitude lower due to the much shorter wavelength. This allows the laser to be focused into a much smaller size, which is of the order of 1 nm.[2] The X-ray FEL is also capable of imaging ultra-small objects and recording ultra-fast events both on atomic and molecular scales. The FEL is required to generate the coherent short-wavelength radiation in the X-ray region. However, the sources for seeding the FEL to produce high-power short-wavelength radiation in the XUV and X-ray regions are not currently available, and therefore other methods are proposed to solve this problem. In one method, the stochastic bunching in the electron beam due to shot noise is exploited.[3] Since the self-amplified spontaneous emission (SASE) starts from the electron beam shot noise, the output of the system typically has limited temporal coherence and relatively large shot-to-shot fluctuation in both power and spectrum, although it does have transverse coherence.[4] In order to improve the longitudinal coherence, methods such as the injection of harmonics generated in gas,[5] the classical or non-classical high-gain harmonic generation,[6−8] and the two-beam FEL for frequency up conversion[9,10] have been proposed. It is shown in Ref. [9] that it is possible to seed the co-propagating electron beams externally at the fundamental resonance of the lower energy electron beam at the longer wavelength, and obtain considerable amplification at the shorter wavelength of the third harmonic of the lower energy beam, which coincides with the fundamental resonance of the higher energy beam.

When the radiation field saturates, the electron beams are trapped by the ponderomotive wave. In one period, the electrons give energy to the radiation, so their energy is reduced. In the next period, they gain energy from the radiation, and therefore the resonance condition is disrupted and the radiation amplitude begins to oscillate. Due to the saturation, the intrinsic efficiency of the FEL is low. To increase the efficiency, we should either decrease the phase velocity of the radiation or accelerate the electrons to compensate the reduced energy of the electron beam.[11,12] To this end, at the saturation point of the third harmonic of the radiation, by decreasing the wiggler amplitude appropriately, the resonance condition of the FEL is restored, which will result in higher intensity XUV and X-ray radiation. The linear reduction in wiggler

†Corresponding author. E-mail: behrouz@aut.ac.ir

© 2012 Chinese Physical Society and IOP Publishing Ltd

amplitude has been studied before.[13] In the present study, the nonlinear reduction in the wiggler field is used.

The purpose of the present study is first to present a non-averaged simulation of the two-beam FEL in the one-dimensional (1D) Compton limit by using Maxwell's equations and the full Lorentz force equation of motion for the electron beams. Second, to study the nonlinear tapering of the magnetic field using the above mentioned method, and third to compare our results with those of the linear reduction in the wiggler amplitude. The effect of tapering on the dynamical stability of the fast electron beam is studied.

In the computational part, we use the simulation technique of Ref. [11]. It needs to be mentioned that in this technique the electron trajectories are not averaged over the wiggler period; therefore the Kroll–Morton–Rosenbluth (KMR) scheme of Ref. [14] is not used. In the KMR method, the average is performed over the Lorentz force equation, and thus only two equations are solved per electron for the energy and the ponderomotive phase.[9,13]

The paper is organized as follows. The model is presented in Section 2, and the fields and dynamical equations are described. In Section 3, the numerical simulations are presented, and the results are illustrated in the diagrams. In Section 4, the effect of tapering and radiation on the dynamical stability of the fast electron beam is studied, and in Section 5, the concluding remarks are made.

2. Model

In this study, a model similar to the one in Refs. [9], [10] and [13] is used. First, we review the model, then the non-averaged equations of the radiation fields and the electron beam equations of motion are defined. In this model, two beams of electrons with different energies copropagating through a magnetic planar wiggler are considered. The electron beam energies are chosen so that the third harmonic of the lower energy beam is at the fundamental resonance of the higher energy beam. The electron beam is bunched when the fundamental resonance field of the lower energy electron beam interacts with the electrons.[10] When the bunching is strong enough, higher harmonics are generated. The result of this nonlinear harmonic generation can be the seeds for the copropagating higher energy electron beam. So the seeding of the higher energy electron beam is not necessary. The coupling of the lower and higher energy beams will lead to the transfer of the properties of the longer wavelength injected seed field to the unseeded shorter harmonic wavelength field. If the Lorentz factors of the lower and the higher energy electron beams are γ_1 and γ_n, respectively, it can be shown from the resonance relation that $\gamma_n = \sqrt{n}\gamma_1$.[9] It needs to be mentioned that the other kind of coupling of the lower and higher energy electron beams in the form of two-stream instability has the potential to degrade the beam quality. However, for the electron beam energies ($\geq$ 500 Mev) and currents ($\geq$ 1 KA) used in the present study, this instability is either below the threshold or has an insignificant effect.[9]

2.1. Field equations

In this section, we give the field equations, which are derived from Maxwell's equations in the 1D Compton limit. The tapered and planar wiggler magnetic fields are described by

$$\boldsymbol{B}_{\rm w}(z) = B_{\rm w}(z)\sin(k_{\rm w}z)\,\widehat{\boldsymbol{e}}_y, \tag{1}$$

$$B_{\rm w}(z) = \begin{cases} B_{\rm w}\sin^2\left(\dfrac{k_{\rm w}z}{4N_{\rm w}}\right), & 0 \leq z \leq N_{\rm w}\lambda_{\rm w}, \\ B_{\rm w}, & N_{\rm w}\lambda_{\rm w} < z, \end{cases}$$

$$\bar{\Omega}_{\rm w}(z) = \begin{cases} \bar{\Omega}_{\rm w0}\,, & \bar{z} \leq \bar{z}_{\rm T1}, \\ \bar{\Omega}_{\rm w0} - m_1(\bar{z} - \bar{z}_{\rm T1}), & \bar{z}_{\rm T1} < \bar{z} \leq \bar{z}_{\rm T2}, \\ \bar{\Omega}_{\rm w}(\bar{z}_{\rm T2}) - m_2(\bar{z} - \bar{z}_{\rm T2}), & \bar{z}_{\rm T2} < \bar{z} \leq \bar{z}_{\rm T3}, \\ \quad\vdots & \\ \bar{\Omega}_{\rm w}(\bar{z}_{\rm T(n-1)}) - m_{(n-1)}(\bar{z} - \bar{z}_{\rm T(n-1)}), & \bar{z}_{\rm T(n-1)} < \bar{z} \leq \bar{z}_{\rm T(n)}, \end{cases} \tag{2}$$

$$\bar{\Omega}_{\rm w}(z) = \begin{cases} \bar{\Omega}_{\rm w0}, & \bar{z} \leq \bar{z}_{\rm T1}, \\ \bar{\Omega}_{\rm w0} - m_1(\bar{z} - \bar{z}_{\rm T1})^2, & \bar{z} > \bar{z}_{\rm T1}, \end{cases} \tag{3}$$

where $\bar{\Omega}_{\rm w0} = eB_{\rm w}/mk_{\rm w}c^2$, $B_{\rm w}$ is the magnetic field for the un-tapered wiggler, $k_{\rm w}$=$2\pi/\lambda_{\rm w}$ is the wiggler wave number, and m_i with $i = 1, 2, \ldots$ are slopes of the lines between $\bar{z}_{{\rm T}i}$ and $\bar{z}_{{\rm T}i+1}$. As described in the previous papers, only the odd harmonic components with $h = 1, 3, \ldots, n$ are considered.[9] If the third harmonic of the lower energy beam is at the fundamental resonance of the higher energy beam, the strongest coupling occurs at $h = n = 3$. The couplings of the higher harmonics are neglected, as their frequencies are not equal to any fundamental resonance. It is shown in Eqs. (2) and (3) that we assume the wiggler amplitude to be a constant up to point $\bar{z}_{\rm T1}$, at which the FEL saturates, and after that $B_{\rm w}$ decreases nonlinearly. The nonlinear variation in wiggler amplitude can be made in two ways. In the first method, the wiggler field is decreased nonlinearly, which is approximated by straight lines with different slopes (Eq. (2)). In the second method, the reduction is parabolic, as shown in Eq. (3).

By using Maxwell's equations and the non-averaged equations of motion of the electron beams, a set of coupled nonlinear differential equations are derived in the slowly varying amplitude approximation. The vector potential and the phase of the plane polarized radiation fields are

$$\delta \boldsymbol{A}_h(z,t) = \sum_h^n \widehat{\boldsymbol{e}}_x[\delta A_h^{(1)} \sin\alpha_{+h} + \delta A_h^{(2)} \cos\alpha_{+h}], \quad (4)$$

$$\alpha_{+h} = h(k_0 z - \omega t), \quad (5)$$

$$\varphi_{+1} = n(k_0 z - \omega t), \quad (6)$$

$$\frac{{\rm d}\alpha_{+h}}{{\rm d}z} = h\left(k_0 - \frac{\omega}{v_{z({\rm low})}}\right), \quad (7)$$

$$\left.\frac{{\rm d}\alpha_{+n}}{{\rm d}z}\right|_{\text{lower energy}} = n\left(k_0 - \frac{\omega}{v_{z({\rm low})}}\right), \quad (8)$$

$$\left.\frac{{\rm d}\alpha_{+n}}{{\rm d}z}\right|_{\text{higher energy}} = \frac{{\rm d}\varphi_{+1}}{{\rm d}z} = n\left(k_0 - \frac{\omega}{v_{z({\rm high})}}\right), \quad (9)$$

where n is the highest harmonic for the low-energy electron beam, which also coincides with the fundamental resonance wavelength of the high-energy electron beam, and$v_{z({\rm low})}$ and$v_{z({\rm high})}$ are the axial velocities of each electron in the lower and higher energy beams. Since the wavelength of interest is less than 1 μm, the collective Raman effects due to the beam space charge wave can be neglected. In the Coulomb gauge, the Maxwell–Poisson equation can be written as[12]

$$\left(\frac{\partial^2}{\partial\bar{z}^2} - \frac{\partial^2}{\partial\bar{t}^2}\right)\left(\sum_{h,{\rm odd}}^n \delta a_h\right) = -4\pi\delta J_x(\bar{z},\bar{t}), \quad (10)$$

where $\delta a_h = e\delta A_h/mc^2$, $\bar{z} = k_{\rm w}z$, $\bar{t} = tk_{\rm w}c$, and $\delta J_x(\bar{z},\bar{t})$ is the current density, which consists of the lower and higher energy electron beams. We can write the current density as an average over the entry time $\bar{t}_0$ at which an electron passes through the $\bar{z} = 0$ plane[12]

$$\tau(\bar{z},\bar{t}_0) = \bar{t}_0 + \int_0^{\bar{z}} \beta_{z,i}^{-1}(\bar{z}',\bar{t}_0)\,{\rm d}\bar{z}', \quad i = \text{low, high}, \quad (11)$$

$$\delta\boldsymbol{J}_i(\bar{z},\bar{t}) = \frac{-\bar{\omega}_{\rm b}^2\beta_{z0,i}}{4\pi} \times \int_{-\infty}^{+\infty} \frac{{\rm d}\bar{t}_0\sigma(\bar{t}_0)\boldsymbol{\beta}_i(\bar{t},\bar{t}_0)\delta\left(\bar{t} - \tau(\bar{z},\bar{t}_0)\right)}{|\beta_{z,i}(\bar{t},\bar{t}_0)|}, \quad i = \text{low, high}, \quad (12)$$

where $\bar{\omega}_{\rm b}^2 = 4\pi n_{\rm b}e^2/mk_{\rm w}^2c^2$, β_{z0} is the initial axial velocity of the electron, $\boldsymbol{\beta}(\bar{t},\bar{t}_0)$ is the velocity of the electron at time $\bar{t}$ which has entered the plane at time $\bar{t}_0$, and $\sigma(\bar{t}_0)$ is the distribution at the entry time. The $\psi_0 = -\bar{\omega}\bar{t}_0$ is the initial pondermotive phase, and the averaging operator is defined as

$$\langle(\cdots)\rangle = \frac{1}{2\pi}\int_{-\pi}^{+\pi} {\rm d}\psi_0\sigma(\psi_0)(\cdots). \quad (13)$$

The slippage is neglected, therefore the system is assumed to be in the steady-state, so the particles that enter the wiggler at times $\bar{t}_0$ separated by integral multiples of the wave period will have identical orbits.[12] Substituting Eq. (4) into wave Eq. (10) and taking its average over one wave period, we derive a set of coupled nonlinear differential equations for δa_h. The field equations for $h < n$ and $h = n$ are, respectively,

$$\left(\frac{\partial}{\partial\bar{z}}\right)\begin{pmatrix}\delta a_h^{(1)}\\ \delta a_h^{(2)}\end{pmatrix} = \frac{\bar{\omega}_{\rm b}^2}{h\bar{\omega}c}\beta_{z0({\rm low})}\begin{pmatrix}\left\langle\frac{u_{x({\rm low})}}{|u_{z({\rm low})}|}\cos\alpha_{+h}\right\rangle\\ -\left\langle\frac{u_{x({\rm low})}}{|u_{z({\rm low})}|}\sin\alpha_{+h}\right\rangle\end{pmatrix}, \quad (14)$$

$$\left(\frac{\partial}{\partial\bar{z}}\right)\begin{pmatrix}\delta a_n^{(1)}\\ \delta a_n^{(2)}\end{pmatrix} = \frac{\bar{\omega}_{\rm b}^2}{(n\bar{\omega})c}\beta_{z0({\rm low})}\begin{pmatrix}\left\langle\frac{u_{x({\rm low})}}{|u_{z({\rm low})}|}\cos\alpha_{+n}\right\rangle\\ -\left\langle\frac{u_{x({\rm low})}}{|u_{z({\rm low})}|}\sin\alpha_{+n}\right\rangle\end{pmatrix} + \frac{\bar{\omega}_{\rm b}^2}{(n\bar{\omega})c}\beta_{z0({\rm high})}\begin{pmatrix}\left\langle\frac{u_{x({\rm high})}}{|u_{z({\rm high})}|}\cos\varphi_{+1}\right\rangle\\ -\left\langle\frac{u_{x({\rm high})}}{|u_{z({\rm high})}|}\sin\varphi_{+1}\right\rangle\end{pmatrix}. \quad (15)$$

The electron beams are assumed to be mono-energetic with their pitch-angle spread being zero, and

the electrons of each beam are considered to have the same initial axial velocities. The current densities of the electron beams are different, so we need to specify the beam current ratio, $R_n = I_n/I_1$. Since the current densities are not equal, the electron beam plasma frequencies of the electron beams will be related by $\bar{\omega}_{bn} = \bar{\omega}_b\sqrt{R_n\gamma_n(\gamma_1^2-1)/\gamma_1(\gamma_n^2-1)}$. Equation (14) shows that A_h with $h < n$ has no direct coupling with the higher energy beam because the higher energy electrons are not resonant with A_h. However, equation (15) demonstrates that the n-th harmonic radiation is driven by both beams, which means that the shorter wavelength radiation extracts energy from both beams and is the superposition of two different types of amplifying radiations, the fundamental resonance of the higher energy beam and the n-th harmonic of the lower energy beam.[9]

2.2. Dynamic equations

In order to complete the formulation, the electron orbit equations should be considered in the presence of fluctuating fields. The Lorentz force equations with the electric and the magnetic fields associated with the vector potentials are used to advance the electrons in z. In the following equations, dimensionless variables $\boldsymbol{u} = \boldsymbol{P}/mc = \gamma\boldsymbol{\beta}$, $\bar{k}_0 = k_0/k_w$, and $\bar{\omega} = \omega/k_w c$ are used.

For the slower electrons of the lower energy beam, the equations are

$$\frac{\mathrm{d}u_{x(\mathrm{low})}}{\mathrm{d}\bar{z}} = \bar{\Omega}_w(\bar{z})\sin(\bar{z}) + \sum_{h,\mathrm{odd}}^{n} h\left(\bar{k}_0 - \frac{\gamma_1\bar{\omega}}{u_{z(\mathrm{low})}}\right) \times (\delta a_h^{(1)}\cos\alpha_{+h} - \delta a_h^{(2)}\sin\alpha_{+h}), \quad (16)$$

$$\frac{\mathrm{d}u_{y(\mathrm{low})}}{\mathrm{d}\bar{z}} = 0, \quad (17)$$

$$\frac{\mathrm{d}u_{z(\mathrm{low})}}{\mathrm{d}\bar{z}} = -\bar{\Omega}_w(\bar{z})\sin(\bar{z})\frac{u_{x(\mathrm{low})}}{u_{z(\mathrm{low})}} - \frac{u_{x(\mathrm{low})}}{u_{z(\mathrm{low})}}\sum_{h,\mathrm{odd}}^{n} h\bar{k}_0 \times (\delta a_h^{(1)}\cos\alpha_{+h} - \delta a_h^{(2)}\sin\alpha_{+h}), \quad (18)$$

$$\frac{\mathrm{d}\alpha_{+h}}{\mathrm{d}\bar{z}} = h\left(\bar{k}_0 - \frac{\bar{\omega}\gamma_1}{u_{z(\mathrm{low})}}\right), \quad (19)$$

$$\left.\frac{\mathrm{d}\alpha_{+n}}{\mathrm{d}\bar{z}}\right|_{\text{lower energy}} = n\left(\bar{k}_0 - \frac{\bar{\omega}\gamma_1}{u_{z(\mathrm{low})}}\right). \quad (20)$$

For the faster electrons belonging to the higher energy beam, the equations are

$$\frac{\mathrm{d}u_{x(\mathrm{high})}}{\mathrm{d}\bar{z}} = \bar{\Omega}_w(\bar{z})\sin(\bar{z}) + n\left(\bar{k}_0 - \frac{\gamma_n\bar{\omega}}{u_{z(\mathrm{high})}}\right) \times (\delta a_n^{(1)}\cos\varphi_{+1} - \delta a_n^{(2)}\sin\varphi_{+1}), \quad (21)$$

$$\frac{\mathrm{d}u_{y(\mathrm{high})}}{\mathrm{d}\bar{z}} = 0, \quad (22)$$

$$\frac{\mathrm{d}u_{z(\mathrm{high})}}{\mathrm{d}\bar{z}} = -\bar{\Omega}_w(\bar{z})\sin(\bar{z})\frac{u_{x(\mathrm{high})}}{u_{z(\mathrm{high})}} - n\bar{k}_0\frac{u_{x(\mathrm{high})}}{u_{z(\mathrm{high})}} \times (\delta a_n^{(1)}\cos\varphi_{+1} - \delta a_n^{(2)}\sin\varphi_{+1}), \quad (23)$$

$$\frac{\mathrm{d}\varphi_{+1}}{\mathrm{d}z} = \left.\frac{\mathrm{d}\alpha_{+n}}{\mathrm{d}z}\right|_{\text{higher energy}} = n\left(\bar{k}_0 - \frac{\bar{\omega}\gamma_n}{u_{z(\mathrm{high})}}\right). \quad (24)$$

Therefore, the nonlinear evolution of the ensemble of electrons having initial phases $-\pi \le \psi_o \le \pi$ is included in the above equations.

In Eqs. (16)–(18), the coupling of the lower energy electrons to the fundamental and the higher harmonic fields is seen. And equations (21)–(23) indicate that the higher energy electrons only couple to the harmonic field A_n.

3. Numerical simulations

In this section, a set of self-consistent first-order differential equations are solved numerically by the fourth-order Runge–Kutta method to demonstrate the evolution of the coupled two-beam FEL system. The initial conditions of the electron beams are chosen so that the electrons are uniformly distributed for $-\pi \le \psi_0 \le \pi$.[11] The steady-state amplifier model is used; therefore, for an un-bunched beam, the initial amplitude of the vector potential, which indicates the amplitude of the injected signal,[11,12] is chosen arbitrarily. The seed field at the third harmonic resonance is two orders of magnitude weaker than that of the longer wavelength field. Therefore, the fundamental resonance of the slow wave can be seeded to up-convert the energy to the higher frequency, leading to the higher power.

By using the tapered magnetic field in Ref. [13], the efficiency was dramatically increased. In that paper, the wiggler field began to decrease linearly at the saturation point. As discussed before, the decline of the wiggler amplitude results in a continuation of the radiation growth by retaining the resonance condition. What disrupted the resonance condition is the reduction of the electron beam energies, but since this reduction can be nonlinear, by reducing the wiggler field nonlinearly, more suitable restoration of the resonance condition can be obtained. Therefore, by using a nonlinearly tapered magnetic field, the harmonic radiation can be amplified further.

The wiggler field amplitude is $B_w = 10.06$ kG, and the wiggler period is $\lambda_w = 3.3$ cm. The length of the entry taper region is $N_w = 10$ wiggler periods, and the seed field at the longer wavelength is $\delta a_1(\bar{z} = 0) \approx 10^{-6}$. A lower energy electron beam with an energy of 470 MeV and a current of 300 A is chosen. An electron beam with an energy of 799 MeV and a current of 600 A is chosen for the fast electron beam. For the parameters, the fundamental resonance takes place at 107.5 nm, and the third harmonic is at 35.8 nm.

It is first assumed that the wiggler amplitude is decreased at $z_{T1} = 22.7$, $z_{T2} = 25.7$, $z_{T3} = 29.3$, $z_{T4} = 32.1$, $z_{T5} = 36.1$, $z_{T6} = 39$, $z_{T7} = 42.5$, $z_{T8} = 45.8$, $z_{T9} = 49.3$, $z_{T10} = 52.1$ (all in meters) with slopes of $m_1 = 0.7 \times 10^{-4}$, $m_2 = 1.2 \times 10^{-4}$, $m_3 = 1.6 \times 10^{-4}$, $m_4 = 2.2 \times 10^{-4}$, $m_5 = 2.6 \times 10^{-4}$, $m_6 = 2.9 \times 10^{-4}$, $m_7 = 3.1 \times 10^{-4}$, $m_8 = 3.3 \times 10^{-4}$, $m_9 = 3.5 \times 10^{-4}$, $m_{10} = 3.9 \times 10^{-4}$, respectively. The evolution of the amplitude of the short-wavelength radiation versus z is plotted for the tapered (solid line) and the un-tapered (dashed line) wigglers in Fig. 1. A substantial growth in the amplitude of the third harmonic for the tapered case is observed. The dash-dotted line in Fig. 1 shows how the normalized amplitude of the wiggler $\Omega_w/k_w c$ varies with z for the nonlinear tapering of the wiggler.

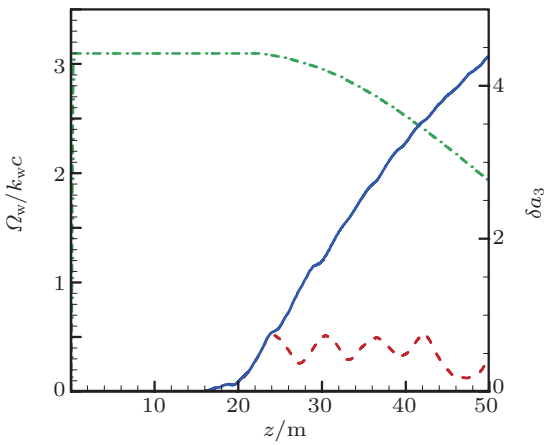


Fig. 1. (colour online) Variation in the amplitude of radiation as a function of z for the third harmonic with nonlinear tapering (solid line). The dashed line shows the intensity of the case with an un-tapered wiggler, and the dash-dotted line shows the variation in $\bar{\Omega}_w$ with z for the nonlinear tapering.

Figure 2 shows the evolution of the amplitude of the third harmonic with z when the parabolic tapering of the wiggler at $z = 22.7$ m and with $m_1 = 1.6 \times 10^{-8}$ is used (solid line). The un-tapered wiggler result is shown by the dotted line. The variation in the normalized wiggler amplitude with z for this parabolic tapering is shown by the dash-dotted line.

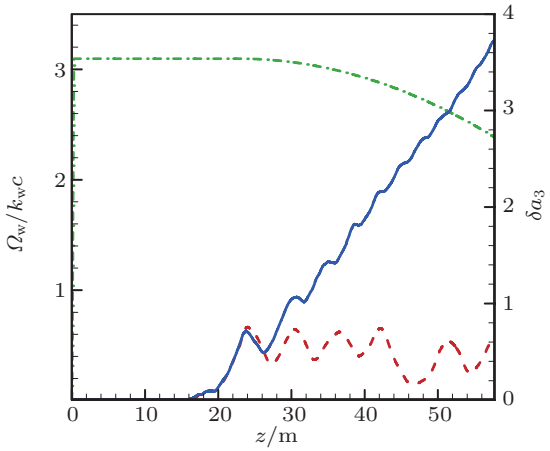


Fig. 2. (colour online) Variation in the amplitude of radiation as a function of z for the third harmonic with parabolic tapering (solid line) $\bar{z}_{T1} = 22.7$ m and $m_1 = 1.6 \times 10^{-8}$. The dashed line shows the amplitude for the case with an un-tapered wiggler, and the dash-dotted line shows the variation of $\bar{\Omega}_w$ with z for the parabolic tapering.

A comparison of the amplifications resulting from the different taperings is shown in Fig. 3. It can be seen that the nonlinear efficiency enhancement resulting from the nonlinear tapering of the wiggler amplitude with different slopes has the highest efficiency.

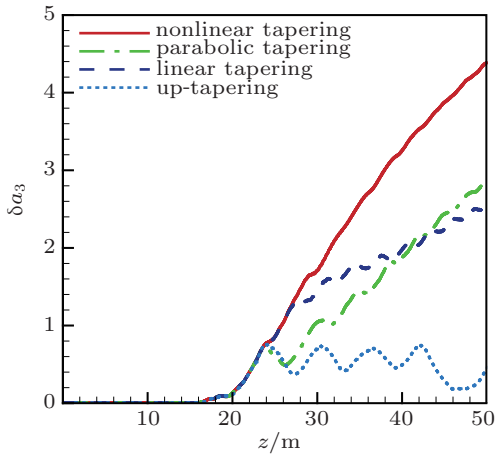


Fig. 3. (colour online) Radiation amplitudes of the third harmonic radiation versus z with un-tapered, linear, parabolic and nonlinear tapering of the wiggler field.

4. The dynamical stability of the electron trajectories

In this section, the effect of the non-linear tapering on the dynamical stability of the electron trajectories of the fast electron beam is studied using the

numerical solution of the Kolmogorov or the metric entropy. This is based on the sensitivity of the motion to small changes in the initial conditions.[15,16] For the regular motion, close neighbor trajectories will separate linearly in time, while they will diverge exponentially for the chaotic motion.

In this procedure, the Kolmogorov entropy is defined by

$$k_N(\tau, x, d) = \frac{1}{\tau N} \sum_{i=1}^{N} \ln \left| \frac{d_i}{d_0} \right|, \tag{25}$$

where N is the number of small time steps τ, $N\tau$ equals the total time T of the motion, $|d_i|$ is the norm or the separation of the two trajectories in the six-dimensional phase space, and $|d_0|$ is the initial value.[16] The value of k_N determines how the trajectories of two neighboring electrons in the phase space diverge from each other. When k_N is small, the separation of the trajectories is small. For positive k_N, the motion is chaotic and close neighbor trajectories separate exponentially. For negative k_N, the motion is regular and the neighbor trajectories approach each other.

A set of first-order ordinary differential equations can be easily derived from the relativistic equations of motion of a single electron in the fields of the wiggler and the radiation.[16] These equations are solved using the fourth-order Runge–Kutta method. The iteration step is 0.035 nm, and the total iteration number is 2×10^9 for an interaction length of 70 m. The reference electron is initially located at $x = 0.0065$ mm with $y = z = 0$. The relativistic factor of the fast electron beam is 1636.8. The neighbor electron is at the same position with a slightly different relativistic factor $1636.8 \times (1+10^{-8})$. Both electrons are assumed to have initial velocities in the axial direction.

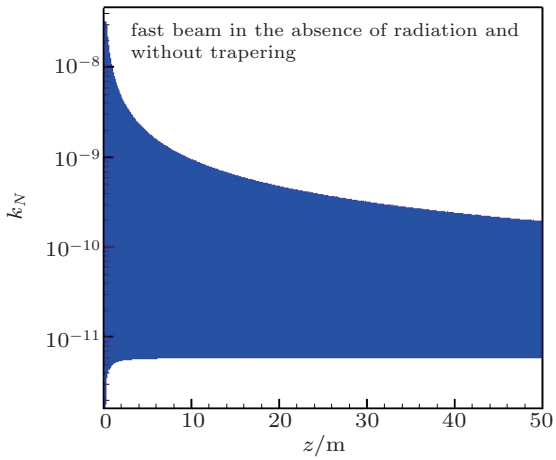


Fig. 4. (colour online) Evolution of Kolmogorv entropy k_N with z for the fast electron beam in the absence of tapering and radiation.

Figure 4 shows the evolution of Kolmogorov entropy k_N of the fast electron beam with z in the absence of tapering and radiation. The k_N rises to 3.2×10^{-8} at around $z = 0.25$ m and falls down to 1.5×10^{-10} at $z = 50$ m. This shows that the motion is regular, which corresponds to the dynamically stable fast electron beam.

The variations of k_N with z for the tapered (solid line) and un-tapered (dotted line) wigglers are shown in Fig. 5. For both cases, k_N oscillates and the smaller amplitude is for the tapered wiggler. This shows that the tapering of the wiggler increases the dynamical stability of the electron motion to some extent.

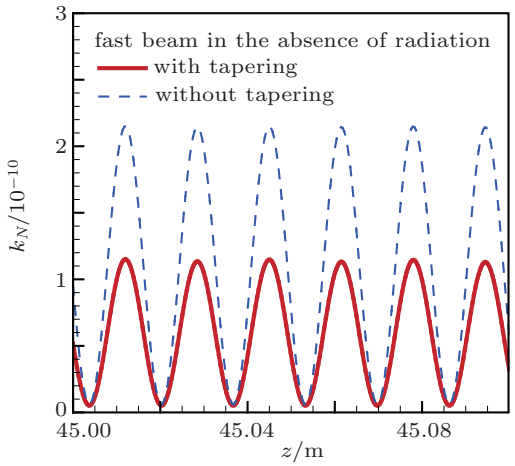


Fig. 5. (colour online) Evolution of Kolmogorv entropy k_N with z for the fast electron beam in the absence of radiation.

The evolution of k_N with z in the presence of the radiation is shown in Fig. 6. It shows that the tapering of the wiggler magnetic field combined with the radiation decreases the dynamical stability by increasing the Kolmogorov entropy.

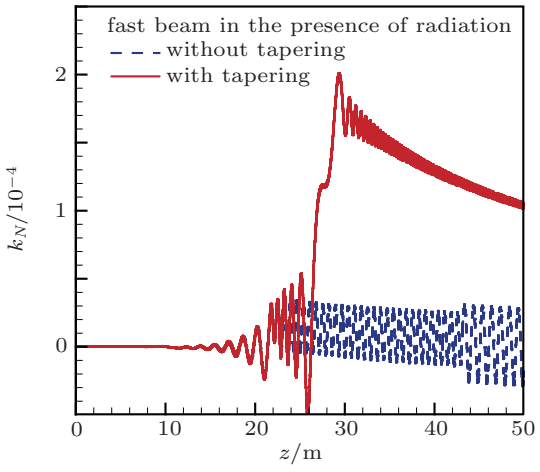


Fig. 6. (colour online) Evolution of Kolmogorv entropy k_N with z for the fast electron beam in the presence of radiation.

5. Conclusion

A non-averaged simulation of the 1D Compton FEL with a nonlinearly tapered planar wiggler is presented in the absence of slippage. By using a two-beam FEL, a source for generating intensified higher harmonics with shorter wavelengths in the XUV and X-ray regions is obtained. By seeding the lower energy beam, considerable seeding of both the harmonic radiation field and the electron bunching of the higher energy beam is possible. Suitably tapering the wiggler amplitude can postpone the saturation of the harmonic radiation, leading to further amplification. In the case of the tapered wiggler, it is found that the nonlinear reduction of the magnetic field can have a larger efficiency enhancement compared to that of linear tapering.

The effect of tapering on the dynamical stability of the motion of an electron in the fast electron beam is also studied. It is found that in the absence of radiation, the tapering of the wiggler magnetic field increases the dynamical stability to some extent. However, the presence of radiation decreases the dynamical stability by increasing the Kolmogorov entropy.

References

[1] O'Shea P G and Freund H P 2001 *Science* **292** 1853

[2] Krishnagopal S, Kumar V, Maiti S, Prabhu S S and Sarkar S K 2004 *Curr. Sci.* **87** 1066

[3] McNeil B 2009 *Nat. Photonics* **3** 375

[4] Singer A, Vartanyants I A, Kuhlmann M, Duesterer S, Treusch R and Feldhaus J 2008 *Phys. Rev. Lett.* **101** 254801

[5] Lambert G, Hara T, Garzella D, Tanikawa T, Labat M, Carre B, Tikamura H, Shintake T, Bougeard M, Inoue S, Tanaka Y, Salieres P, Merdji H, Chubar O, Gobert O, Tahara K and Couprie M E 2008 *Nat. Phys.* **4** 296

[6] Yu L H, Babzien M, Ben-Zvi I, DiMauro L F, Doyuran A, Graves W, Johnson E, Krinsky S, Malone R, Pogorelsky I and Skaritka J 2000 *Science* **289** 932

[7] Xiang D and Stupakov G 2009 *Phys. Rev. ST Accel. Beams* **12** 030702

[8] Stupakov G 2009 *Phys. Rev. Lett.* **102** 074801

[9] McNeil B W J, Robb G R M and Poole M W 2004 *Phys. Rev.* E **70** 035501

[10] Rouhani M H and Maraghechi 2010 *Phys. Rev. ST Accel. Beams* **13** 080706

[11] Rouhani M H and Maraghechi B 2009 *Phys. Plasmas* **16** 093110

[12] Freund H P and Antonsen J M 1996 *Principles of Free Electron Laser* (2nd Edn.) (London: Chapman and Hall) Chap. 5

[13] Rouhani M H, Maraghechi B and Saberi H 2009 *Phys. Plasmas* **16** 123105

[14] Kroll N M, Morton P L and Rosenbluth M N 1981 *IEEE J. Quantum Electron* **17** 1436

[15] Tabor M 1989 *Chaos and Integrability in Nonlinear Dynamics* (New York: Wiley)

[16] Salehi E, Maraghechi B and Rouhani M H 2010 *Phys. Plasmas* **17** 113102